Influence of fracture orientation distribution function on the estimates of gas-hydrate saturation of site 10 at Krishna-Godavari Basin, India

Yudhvir Singh[1], Rajesh R Nair[1*]

[1]Department of Ocean Engineering, Indian Institute of Technology Madras, Chennai,

India

*Corresponding author

Abstract

We estimate the gas-hydrate saturation in fractured reservoirs of gas hydrate-rich marine sediments from Krishna-Godavari basin along the eastern margin of India. Effective medium modeling (EMM) is a combination of self-consistent approxi-mation (SCA), differential effective medium (DEM) modeling and smoothing and ideals with the anisotropy associated with clay platelets' orientation. It proves to be a good choice attributable to its dependency on physical parameters alone. Previous approaches appertain to the implementation of orientation distribution function (ODF) on clay platelets alone assuming a vertical ellipsoidal shape of gas hydrates whilst in the present study, we have implemented ODF on hydrate bearing fractures assigning an ellipsoidal shape to them as well. A bias of ~2-4% in the saturation estimates streamlines the betterness of this approach.

I. INTRODUCTION

Gas hydrates are clathrates composed of water molecules and natural gas (primarily methane), stable at low temperature, high pressure and format favorable solubility conditions for gas. The narrow range of pressure - temperature for hydrate stability and abundant supply of natural gas, govern natural gas hydrates' distribution, which are most often found in outer shallow continental margins and permafrost regions [Kvenvolden 1993, Sloan 1998, Kvenvolden and Lorenson 2001, Thakur, N.K. and Rajput, S. 2011]

National Gas Hydrate Program (NGHP), formulated by Indian government in 1996 to explore gas hydrate resources in India, found one of the richest deposits of gas hydrates in the clay-rich marine deposits of Krishna-Godavari (KG) Basin (Figure 1), along the eastern continental margin of India. During the first expedition (NGHP-01), in the year 2006, a total of 39 holes were drilled at 21 sites and the gas hydrate deposits were spotted at 13 sites. Site 10 (NGHP-01-10) was found to be the richest in terms of gas hydrate accumulation [Collett et al. 2008]. At site 10, coring, logging while drilling (LWD) and wireline logging were performed within few meters of depth and it was reported that gas hydrates are present within 25-160 m below seafloor (mbsf) [Collett et al. 2008]. Gas hydrate morphologies can be pore-filling and grain-displacing, where pore filling hydrates can be load bearing (contact model) or non-load bearing (non-contact model) depending upon whether they are connected or isolated in pores [Chand et al. 2004, Holland et al. 2008, Ghosh et al. 2010]. The LWD borehole resistivity-at-bit (RAB) image of hole 10A (Latitude: 15° 51.86' N; Longitude: 81° 50.07' E) exposed massive gas hydrates, commonly occurring in fractures of clay-rich sediments [Collett et al. 2008, Cook and Goldberg 2008, Ghosh et al. 2010]. X-ray computed tomographic (CT) images of core recovered from hole 10B (~10m distant from 10A) suggested that gas hydrates are in form of solid nodules, veins and high-angle fracture fills [Collett et al. 2008, Holland et al. 2008]. Cook et al. [2010] and Rees et al. [2011] converge towards a relative random fracture orien-tation by plotting the projection of equal-area lower-hemisphere of fractures in well 10A and 10B. The studies further claim that the fractures tend to align at high angle, between 50-90°, in majorities of holes that underwent investigation. Considering the above studies, it

can be assumed that the fractures at site 10 are partially aligned in vertical direction.

Figure 1. Location map of the study area

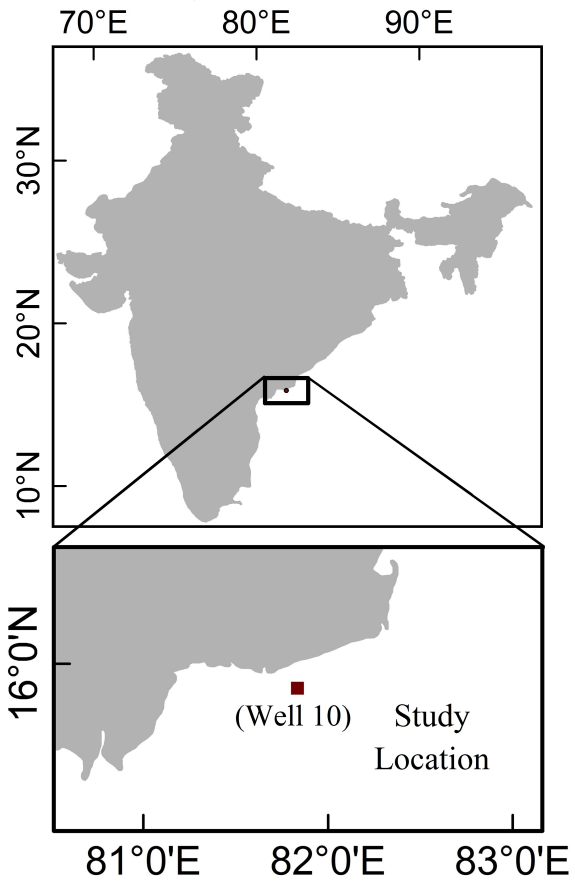

Clay-rich sediments are anisotropic by nature due to clay platelets orientation that depends on the size and shape of platelets as well as on depositional history and geological environment [Hornby et al. 1994, Sayers 1994]. Clay deposits can show transverse isotropy as in most cases, clay platelets have preferred horizontal alignment i.e. clay platelets have (in most cases) symmetric orientation distribution function about vertical direction [Bennett et al. 1991]. Jakobsen et al. [2000] used a hypothetical orientation distribution function for clay-rich sediments, making sediments transverse isotropic, to find elastic properties of gas hydrate bearing sediments.

Numerous rock physics theories have come up relating seismic velocities with the sediment morphology and gas hydrate saturation. A plethora of authors (Miller et al., 1991; Hyndman and Spence, 1992; Dvorkin and Nur, 1993; Wood et al., 1994; Lee et al., 1996; Ecker et al., 1998; Guerin et al., 1999; Helgerud et al., 1999; Jakobsen et al., 2000; Gei and Carcione, 2003) applied a number of rock physics theories to compute gas hydrate saturation assuming uniform, isotropic and pore-filling morphologies. Some other methodologies are based on semi empirical formulae where a weighing factor or an arbitrary constant comes into picture which has to be fixed initially. For instance, a combination of time average equation [Wyllie et al. 1958] and wood equation [Wood 1941] is used by Lee et al. [1996] adding a weighing factor and a constant to simulate the rate of lithifaction with hydrate concentration. Jakobsen et al. [2000] made use of an effective medium modeling, to compute gas hydrate saturation at Blake Ridge (South-Eastern U.S. Continental Margin). It is based on physical parameters and considers the anisotropy of clay through an orientation distribution function (ODF) of clay platelets'.

In the present study, a combined approach of self-consistent approximation (SCA) [Willis 1977], differential effective medium (DEM) theory [Nishizawa 1982] and first order smoothing approximation [Frisch 1968] towards the computation of clay platelets' distribution is used. The above approach is further used for gas hydrate saturation measurements associated with various morphologies of hydrates [Jakobsen et al. 2000; Chand et al. 2004; Chand et al. 2006; Ghosh et al. 2010]. Effective medium modeling [Jakobsen et al. 2000] is capable of calculating elastic properties of isotropic as well as transverse isotropic gas-hydrate bearing sediments and ODF is implemented on clay platelets. Ghosh et al. [2010] used effective medium modeling to calculate gas hydrate saturation at well 10D, corresponding to three different morphologies. In this approach, we emphasize on how ODF is implemented on fractures and have focused on its influence in pushing the precision in the estimates towards the higher side.

X-ray computed tomographic (CT) images advocates high-angle fractures, on other hand, projection of equal-area lower-hemisphere

suggests a relative random orientation of fractures in site 10 [Collett et al. 2008, Holland et al. 2008, Cook et al.2010, Rees et al. 2011]. Hence, implementing ODF on hydrate-filled fractures, preferably aligned in vertical direction is one step forward. In present study we estimated hydrate saturation for well 10A and 10D, considering fractures filled with hydrates as well as for combined approach (pore filling +fractures) incorporating fracture orientation distribution function (ODF).Cracks/fractures are assumed ellipsoidal in shape and embedded in host and the effective elastic tensor of aggregates was calculated using Nishizawa [1982] approach [Ghosh et al. 2010]. Method of Grechka and Tsvankin [2004] was used to rotate the fractures. The compliance matrix of a medium is separated into fracture compliance matrix and background materials compliance matrix. Then, the fracture compliance is rotated via bond transformation [Winterstein 1990]. Finally the background material compliance and fracture rotated compliance are added to get the compliance of effective medium with oblique/vertical fracture.

II. METHODOLOGY

Effective medium modeling was developed following the approach used by Hornby et al. [1994] and Sheng [1990] in which self-consistent approximation (SCA) [Willis 1977] was incorporated along with differential effective medium (DEM) theory [Nishizawa 1982]followed by smoothing of aggregates[Frisch 1968]. In SCA, a single inclusion having comparatively infinitesimal volume goes in host having the elastic properties of effective medium (yet to be determined), and the process continues until the desired volume of inclusion material is achieved. SCA loses bi-connectivity except the porosity stays within 40-60% [Berryman 1980, Hornby et al. 1994] so to maintain the bi-connectivity a combined approach of SCA and differential effective medium modeling (DEF) is used in which first effective medium is generated using SCA (within the range of 40-60% porosity), then successively removing the infinitesimal sub-volume of host material and replacing it with a corresponding sub-volume of pore fluid [Hornby et al. 1994, Jakobsen et al. 2000]. A combination of SCA and DEM provides the elastic properties of effective medium for desired porosity.

The edge effects due to the orientation of individual platelets are minimized by calculating Voigt [1928] average followed by a 'method of smoothing' [Bonilla and Keller 1985]. Locally aligned clay platelets together with pore fluid are averaged for their ODF.ODFs of locally aligned clay platelets together with pore fluids are averaged by Voigt [1928] averaging technique in which the clay platelets are successively rotated through desired angles and their ODFs are averaged. Hornby et al. [1994] explained the above process in these steps: for each angle (θ) specified by ODF, the effective tensor of stiffness for the aligned clay fluid composite is rotated along one of the horizontal axis by θ and then made symmetric with respect to the vertical axis of symmetry by a series of successive rotations of $\pi/3$ and averaging the result. Then finally rotated stiffness tensor for all rotated domains are averaged over θ and weighted according to D(θ) where D(θ) is normalized distribution function of clay platelets (see equation 1).

$$c^{v} = \frac{1}{6}\sum_{n=1}^{N}\sum_{i=1}^{6} D(n)c^{*}(n,\varphi_i) \qquad (1)$$

where c^v is the effective stiffness of whole composite, n in D(n) stands for discrete angles, $c^*(\theta, \varphi)$ is the tensor of effective stiffness for the aligned clay-fluid sub-composites whose symmetry axis is rotated by the polar angles θ relative to vertical and φ is azimuthal angle. The notations in the equation are same as used by Hornby et al. [1994]. To further improve the results, methods of smoothing [Frisch 1968; Gubernatis and Krumhansl 1975; Bonilla and Keller 1985; Sheng 1995] is applied. Sayers [1994] developed an alternate and simpler way to perform Voigt averaging by providing the tow non-zero constants, W_{200} and W_{400} (others are zero in the case of transverse isotropy) in terms of generalized Legendre functions.

From modeling point of view, non-load bearing hydrate modeling is achieved by starting SCA with clay and water and then replacing

water with hydrates through DEM. In load-bearing the sequence of water and hydrate is interchanged [Chand et al. 2004; Chand et al. 2006; Ghosh et al. 2010]. Silt and other particles (if present) can be added later via DEM approach in sub-composite of clay, water and hydrate.

In fine grain sediments, gas hydrates can create and occupy veins and fractures apart from residing in pores [Malone 1985; Kvenvolden 2000; Kvenvolden 1994; Chand et al. 2004]. In this study, fractures/veins are assumed as ellipsoids filled with hydrates and embedded in clay, quartz, water and pore-hydrate composites [Ghosh et al. 2010]. In grains displacing morphology, hydrates embedded as ellipsoids force apart the matrix composed of clay, quartz, water and pore-hydrates (if present) [Chand et al. 2004; Holland et al. 2008; Ghosh et al. 2010]. In such environments where hydrates are in pore as well as in fractures, a combined approach of pore-filling and grain-displacing can be applied.

1. Inclusion of fractures with ODF

Here, fractures/veins are considered as ellipsoids filled with hydrate, whose aspect ratio varies from 0.001 (thin vein) to 1.0 (nodule) [Collett et al. 2008; Ghosh et al. 2010]. Fractures with ODF can be embedded through effective medium modeling, by two different ways depending upon their ODF. First one is simple and easy to implement and works in case if the ODFs of fractures and clay platelets are identical. In this approach, fractures are embedded in individual sub-composite of clay, quartz, water and pore-hydrates prior to Voigt [1928] averaging. The volume of hydrate-filled fracture in each sub-composite should be equal to the desired volume/fraction. Suppose in a case, where the fracture porosity is 10% of total rock volume in that case in each sub composite of clay and quartz, we can add 10% fractures (filled with hydrates in this case)of the total volume and then rotate. Once fracture is embedded, then during rotation via bond transformation [Winterstein 1990] of each domain (fracture+sub-composite), fracture undergoes the same rotation and, as a result we achieve the desired ODF for fracture in sediments. In this approach averaging can also be achieved by Sayers' [1994] simplified approach if W_{200} and W_{400} are known. A schematic diagram of clay sub-composite embedded with vertically oriented ellipsoidal hydrates, prior to averaging and smoothing, is shown in figure 2.

Figure 2 (a) Schematic diagram of clay sub-composite embedded with hydrate-filled fractures approximated as ellipsoid for effective medium modeling. **(b)** Two

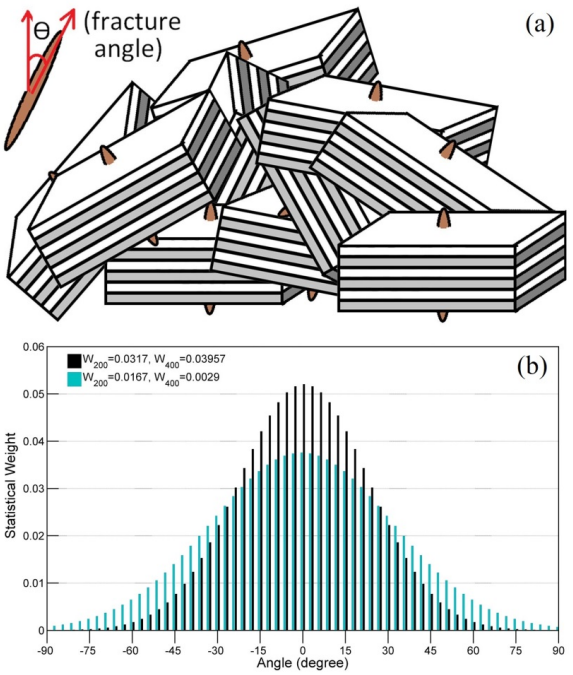

ODF for clay platelets. ODF with W_{200}=0.0167 and W_{400}=0.0029 is used by Jakobsen et al. [2000] and ODF with W_{200}=0.0317 and W_{400}=0.03957 is estimated and used by Ghosh et al. [2010] for gas hydrate saturation measurements for well 10D for KG basin. In this study we use latter as ODF of clay as well as of fractures.

In another approach, if the ODF of fractures and clay-platelets are different, in this case total porosity of fractures filled with hydrate is achieved by controlling the volume of fractures to be embedded, in each sub-composite prior to averaging and smoothing. Volume of each ellipsoid filled with fracture hydrate in respective sub-composite is orientation's angle (θ) dependent controlled by ODF of fracture and clay.

For example, to embed a total of 10% of hydrate-filled fractures, if normalized statistical weight of clay platelets at 60°with horizontal is 0.10 and of hydrate-filled fracture is 0.12, then at this particular angle, volume of hydrate should

be included as (0.12/0.10)×10=12% and during averaging, ODF of clay should be used. If h_{fa} is the overall saturation in fracture to be achieved in sediments, $D_f(n)$ is normalized discrete distribution function of fractures, $D_c(n)$ is distribution function of clay platelets, $h_f(n)$ is hydrate volume/frac-tion to be embedded at particular angle (n), then $h_f(n)$ can be represented in the form of other variables as

$$h_f(n) = \frac{D_f(n)}{D_c(n)} h_{fa} \qquad (2)$$

Once each domain is ready with vertical fractures of volume as defined by equation (2), each domain is rotated through angle defined by denominator's ODF (in this clay ODF) and averaged using Voigt averaging, followed by smoothing. To toggle between W_{200} and W_{400}, required for Sayers' [Sayers 1994] approach and statistical weight of discrete angles, required for Voigt averaging [Voigt 1928], one can follow the methodology adopted by Johansen et al. [2004]. Figure (2 b) shows two different orientation distribution functions for clay platelets. ODF with W_{200}=0.0167 and W_{400}=0.0029 is used by Jakobsen et al. [2000] and ODF with W_{200}=0.0317 and W_{400}=0.03957 is estimated and used by Ghosh et al. [2010] for gas-hydrate saturation measurements for well 10D of KG basin.

III. RESULTS AND DISCUSSIONS

Gamma ray, density, resistivity and acoustic P-wave logs of well 10A were acquired through LWD while gamma ray, density, acoustic P-wave and S-wave logs of well 10D were acquired through wireline logging [Collett et al. 2008]. Site 10 is nano fossil-rich clay where the mineralogy estimated from core data is 95% clay and 5% silt on average [Collett et al. 2008, Ghosh et al. 2010]. In the present study, ODF of fractures is assumed the same as of clay platelets, where W_{200} =0.0317 and W_{400}=0.03957 are used [Ghosh et al. 2010] for the purpose of averaging. The values of density (ϱ), bulk moduli (K), shear moduli (μ) used in this study have been shown in Table 1.

Constituent	K(GPa)	μ (GPa)	ϱ (g/cm^3)
Clay	21.20	6.66	2.60
Quartz	37.79	44.07	2.70
Water[a]	2.25	0	1.03
Hydrate[b]	8.27	3.49	0.92

[a]Density of water from Collett et al. [2008];
[b]Values for Hydrate are from Helgerud et al.[2009]

Table 1. Bulk moduli (K), shear moduli (μ), densities (ϱ) used in this study [Jakobsen et al. 2000]

Here, SCA (50% porosity) is combined with DEM to establish bi-connectivity for clay-water composite followed by inclusion of quartz as isolated phase through DEM. Then fractures are included as hydrate ellipsoids, having aspect ratio = 0.001, removing matrix and pore-fluid in such a way that final composite is an aggregate of all. This is followed by averaging and smoothing to consider the effect of clay, fracture orientation and to remove edge effects, respectively. Starting with isotropic background (aspect ratio for clay platelets is 1), we calculated the sonic velocity (V_P) as a function of increasing hydrate saturation, due to fractures filled with hydrates. Figure 3(a toc) shows modeled V_P associated with horizontal and vertical fractures and for fractures with ODF corresponding to three different porosities φ=73.7, φ =62 and φ =57. Figure 3(d to f) shows the effect of fracture rotation on velocity.

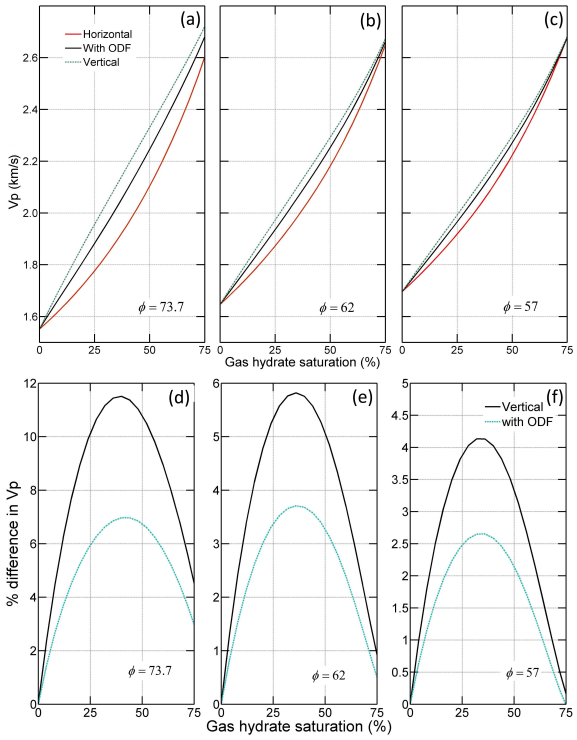

Figure 3. (a to c) Variations of V_P with hydrate saturation in fractures with three porosities and aligned in horizontal, vertical and preferably oriented in vertical direction with ODF. (d to f) Percent difference in calculated V_P for purely vertical and fractures with ODF with respect to horizontal fractures.

Effect of rotation is more for higher porosities and intermediate saturations and decreases as porosity decreases. About 4% difference is observed when saturation is calculated for purely vertical fractures or for fractures rotated with ODF. We estimated gas hydrate saturation in both the wells for contact (load-bearing) and non-contact (non-load bearing) modes of pore filling morphologies. Figure 4 shows hydrate saturation estimates of well 10A and 10D with isotropic and anisotropic (more precisely, transverse) background. Anisotropy is achieved using an aspect ratio of 1:20 for clay platelets and pore fluids [Jakobsen et al. 2000] during SCA and DEM modeling. For well 10D, maximum hydrate saturation estimated for anisotropic non-contact model, at ~67 mbsf, is 58% which is ~2% more than that was calculated by Ghosh et al. [2010], and this may be due to different elastic moduli of hydrates taken into consideration.

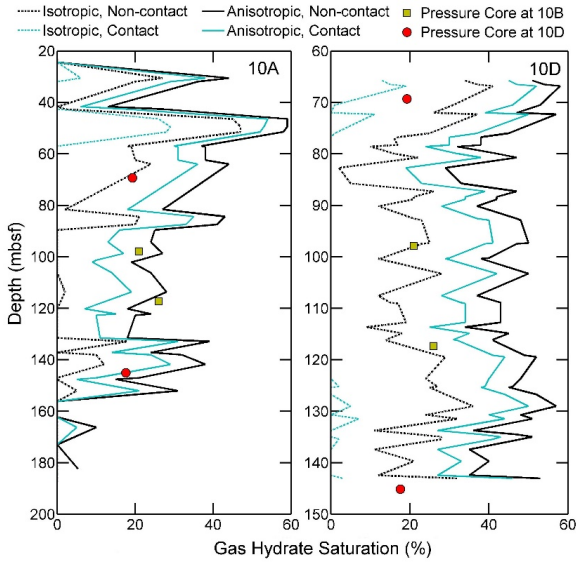

Figure 4. Gas hydrate saturation for well 10A and 10D in case of pore filling morphology. Saturation measured via pressure core also shown for well 10D and 10B (within ~10m distance to 10A) [Collett et al. 2008, Lee and Collett 2009].

We found 52%, 41%, and 19% hydrate saturation for anisotropic contact, isotropic non-contact and isotropic contact models, respectively. For well 10A, maximum hydrate saturation estimated is 59%, 54%, 47% and 29% for pore filling morphologies modeled as anisotropic non-contact, anisotropic contact, isotropic non-contact and isotropic contact, respectively. Each depth point is given a normalized weight proportional to its total distance from lower and upper depth points during averaging, as all points are not equally spaced. Average hydrate saturation is 50%, 41%, 24%, ~1% for 10D and 25%, 18%, 8%, ~1% for 10A, in anisotropic non-contact, anisotropic contact, isotropic non-contact and isotropic contact morphologies, respectively.

Further, figure 5 shows gas hydrate saturation for wells 10A and 10D if hydrates are present in fractures. Three different scenarios have been taken into consideration for fractures, first if all fractures are vertical, second if fractures are oriented as ODF, third if fractures have ODF

but are fixed to 20% of the total porosity. In modeling, all fractures are considered to be filled with hydrates.

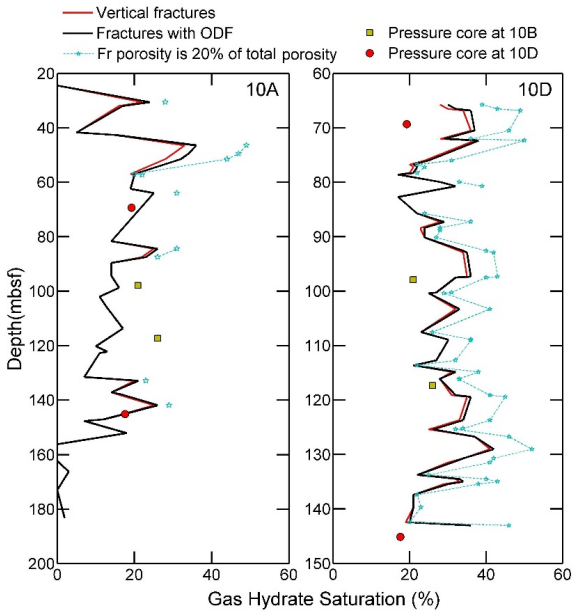

Figure 5. Gas hydrate saturation varying with depth is depicted for well 10A and 10D. Red (light line) represents grain displacing morphology if fractures are vertical. Black (dark line) represents saturation variation with depth for fractures oriented and smoothed according to ODF. Dotted and/or star represents hydrate saturation for combined approach of pore filling and grain displacing if fractures porosity contribute to 20% to the total porosity.

When estimated for fractures with and without ODF, saturation goes to a maximum of 41% and 42% for well 10D and 33% and 36% for well 10A, respectively, while average saturation is 28% and 29% for well 10D and 14% and 13% for well 10A. For fracture porosity limited to 20% of total porosity (combined morphology), maximum observed hydrate saturation is 52% and 49% for well 10D and 10A, respectively. It should be noted that if hydrate saturation is less than 20% which means hydrate filled fracture porosity considered should be less than 20%, so in this case saturation can be limited to saturation observed for grain displacing morphology i.e. dark black line in figure 4.

Lee and Collett [2009] estimated a maximum of 44% saturation at 10D through anisotropic P-wave modeling while it was 21% from observed S-wave velocity following approach of White [1965]. Maximum calculated saturation from Archie's [1942] equation using higher n and m parameters, corresponding to anisotropic condition in well 10A is ~70%. At10A, recorded P-wave velocity may be less than the actual value due to dissociation of gas during LWD in gas hydrate interval [Lee and Collett 2009]. This may be one reason of underestimating gas hydrate saturation at 10A when compared to core data. At 10D, though estimated hydrate saturation for filled fracture is on the higher side when compared to core data, [Lee and Collett 2009] up to 4% underestimation is permissible. Numerical studies point out that the hydrate reservoir is complex and even fluid flow could alter the geomechanical characteristics of reservoir [Kim et al. 2012], and hence outcome of logs.

IV. CONCLUSIONS

Effective medium modeling for hydrate saturation via SCA, DEM and smoothing depends on physical parameters and implementing ODF on fractures can be considered as an improvement in the method. At site 10, it is observed that two approaches, all vertical fractures or fractures with ODF, differ by ~2-4% in hydrate saturation estimates. Further, it can be concluded that the difference in velocity calculated by forward modeling (which in turn is saturation measured by inverse modeling) is higher for high porosities and it is maximum if hydrate saturation is ~35-45% [Figure 3].

REFERENCES

Archie, G.E. (1942), The electrical resistivity log as an aid in determining some reservoir characteristics, J. Pet. Technol., 1, 55–62.

Bennett, R.H., W.R. Bryant, and M.H. Hulbert (1991), Microstructure of Fine-Grained Sediments: From Mud to Shale, Springer-Verlag, New York.

Berryman, J.G. (1980), Long wavelength propagation in composite elastic media I: Spherical inclusions, J. Acoust. Soc. Am., 68, 1809-1819.

Bonilla, L.L., and J.B. Keller (1985), Acoustoelastic effect and wave propagation in heterogeneous

weakly anisotropic materials, J. Mech. Phys. Solids, 33, 241–261.

Chand, S., T.A. Minshull, D. Gei, and J.M. Carcione (2004), Elastic velocity models for gas hydrate-bearing sediments-a comparison, Geophys. J. Int., 159, 573–590.

Chand, S., T.A. Minshull, J.A. Priest, A.I. Best, C.R.I. Clayton, and W.F. Waite (2006), An effective medium inversion algorithm for gas hydrate quantification and its application to laboratory and borehole measurements of gas hydrate-bearing sediments, Geophys. J. Int., 166, 543–552.

Collett, T.S., M. Riedel, J. Cochran, R. Boswell, J. Presley, P. Kumar, A.V. Sathe, A.K. Sethi, M. Lall, V.K. Sibal, NGHP Expedition 01 Scientists (2008), NGHP Expedition 01 (2006), Initial Reports, Directorate General of Hydrocarbons, Noida and Ministry of Petroleum & Natural Gas, India. 4 volumes.

Cook, A., and D. Goldberg (2008), Stress and gas hydrate-filled fracture distribution, Krishna-Godavari basin, India, Proceedings, 6th International Conference on Gas Hydrates, Vancouver, B.C., Canada, July 6–10.

Cook, A.E., B.I. Anderson, A. Malinverno, S. Mrozewski, and D.S. Goldberg (2010), Electrical anisotropy due to gas hydrate-filled fractures, Geophys., 75(6), F173-F185.

Dvorkin, J., and A. Nur (1993), Rock physics for characterization of gas hydrates: The future of energy gases, USGS Prof. Paper 1570, U.S. Geological Survey, Washington, D. C.

Ecker, C., J. Dvorkin, and A. Nur (1998), Sediments with gas hydrates: Internal structure from seismic AVO, Geophys., 63, 1659–1669.

Frisch, U. (1968), Wave propagation in random media, in Probabilistic Methods in Applied Mathematics, vol. 1, edited by A.T. Bharucha-Reid, pp. 75-198, Academic, San Diego, California.

Gei, D., and J.M. Carcione (2003), Acoustic properties of sediments saturated with gas hydrate, free-gas and water, Geophys. Prospect., 51, 141–157.

Ghosh R., K. Sain, M. Ojha (2010), Effective medium modeling of gas hydrate-filled fractures using the sonic log in the Krishna-Godavari basin, offshore eastern India, J. Geophys. Res, 115, B06101.

Grechka, V., and I. Tsvankin (2004), Characterization of dipping fractures in a transversely isotropic background, Geophys. Prospect., 52, 1–10.

Gubernatis, J.E., and J.A. Krumhansl (1975), Macroscopic engineering prop-erties of polycrystalline materials: Elastic properties, J. Appl. Phys., 46, 1875-1833.

Guerin, G., D. Goldberg, and A. Meltser (1999), Characterization of in situ elastic properties of gas hydrate-bearing sediments on the Blake Ridge, J. Geophys. Res., 104, 17,781–17,795.

Helgerud, M.B., J. Dvorkin, A. Nur, A. Sakai, and T. Collett (1999), Elastic wave velocity in marine sediments with gas hydrates: Effective medium modeling, Geophys. Res. Lett., 26, 2021-2024.

Helgerud, M.B., W.F. Waite, S.H. Kirby, and A. Nur (2009), Elastic wave speeds and moduli in polycrystalline ice Ih, sI methane hydrate, and sII methane-ethane hydrate, J. Geophys. Res., 114, B02212.

Holland, M., P. Schultheiss, J. Roberts, and M. Druce (2008), Observed gas hydrate morphologies in marine sediments, Proceedings, 6th International Confe-rence on Gas Hydrates, Vancouver, B.C., Canada, July 6–10.

Hornby, B.E., L.M. Schwartz, and J. A. Hudson (1994), Anisotropic effective medium modeling of the elastic properties of shales, Geophys., 59, 1570–1583.

Hyndman, R.D., and G.D. Spence (1992), A seismic study of methane hydrate marine bottom simulating reflectors, J. Geophys. Res., 97, 6683–6698.

Jakobsen, M., J.A. Hudson, T.A. Minshull, and S.C. Singh (2000), Elastic properties of hydrate-bearing sediments using effective medium theory, J. Geophys. Res., 105, 561–577.

Johansen T.A., B.O. Ruud, and M.Jakobsen (2004), Effect of grain scale alignment on seismic anisotropy and reflectivity of shales, Geophys. Prospect., 52, 133-149.

Kim, J., G. Moridis, D. Yang, and J. Rutqvist (2012), Numerical Studies on Two-Way Coupled Fluid Flow and Geomechanics in Hydrate Deposits, SPE Journal, 17(02), 485-501.

Kvenvolden, K.A. (1993), Gas hydrates-geological perspective and global change, Rev. Geophys., 31(2), 173-187.

Kvenvolden, K.A., (1994), Natural Gas Hydrate Occurrence and Issues, Annals of the New York Academy of Sciences. 715(1), 232-242

Kvenvolden, K.A., (2000), Natural gas hydrate: introduction and history of discovery in Coastal System and Continental Margins, Natural Gas Hydrate in Oceanic and Permafrost Environments, 9-16, ed. Max, M.D., Kluwer Academic Press, Dordrecht.

Kvenvolden, K.A., and T.D. Lorenson (2001), The global occurrence of natural gas hydrate, in Natural Gas Hydrates: Occurrence, Distribution,

and Detection, Geophys. Monogr. Ser, vol. 124, edited by C. K. Paull and W. P. Dillon, 3–18, AGU, Washington, D. C.

Lee, M.W., D.R. Hutchinson, T. S. Collett, and W. P. Dillon (1996), Seismic velocities for hydrate-bearing sediments using weighted equation, J. Geophys. Res., 101, 20,347–20,358.

Lee, M.W., Collett, T.S. (2009), Gas hydrate saturations estimated from fractured reservoir at Site NGHP-01-10, Krishna-Godavari Basin, India,J. Geophys. Res., 114, B07102.

Malone, R.D. (1985), Gas hydrates, DOE Topical Rep. DOE/METC/Rep. DOE/METTC/SP-218(DE85001986):35, Dep. of Energy, Washington, D. C.

Miller, J. J., M.W. Lee, and R. VonHuene (1991), An analysis of a seismic reflection from the base of a gas hydrate zone, offshore Peru, American Association of Petroleum Geologists Bulletin, 75, 910–924.

Nishizawa, O. (1982), Seismic velocity anisotropy in a medium containing oriented cracks: Transversely isotropic case, J. Phys. Earth, 30, 331–347.

Rees, E.V.L., J.A. Priest, and C.R.I. Clayton (2011), The structure of methane gas hydrate bearing sediments from the Krishna-Godavari Basin as seen from Micro-CT scanning, Mar. Pet. Geol., 28, 1283-1293.

Sayers, C.M. (1994), The elastic anisotropy of shales, J. Geophys. Res., 99, 767–774.

Sheng, P. (1990), Effective medium theory of sedimentary rocks, Phys. Rev. B, 41, 4507–4512.

Sheng, P. (1995), Introduction to Wave Scattering, Localization and Mesoscopic Phenomena, Academic, San Diego, California.

Sloan, E.D. (1998), Clathrate Hydrate of Natural Gases, Marcel Dekker, New York.

Thakur, N.K. and Rajput, S. (2011). Exploration of Gas Hydrates, Springer-Verlag, Berlin Heidelberg, doi: 10.1007/978-3-642-14234-5, 277

Voigt, W. (1928), Lehrbuch der Kristallphysik: Teubner, Leipzig.

White, J.E. (1965), Seismic Waves—Radiation, Transmission, and Atten-uation, 320, McGraw-Hill, New York.

Willis, J.R. (1977), Bounds of self-consistent estimates for the overall properties of anisotropic composites, J. Mech. Phys. Solids, 25, 185–202, doi:10.1016/0022-5096(77)90022-9.

Winterstein, D.F. (1990), Velocity anisotropy terminology for geophy-sicists, Geophys. 55, 1070–1088.

Wood, A.B. (1941), Text Book of Sound, 578, Macmillan, Indianapolis, Ind.

Wood, W.T., P.L. Stoffa, and T.H. Shipley (1994), Quantitative detection of methane hydrate through high resolution seismic velocity analysis, J. Geophys. Res., 99, 9681–9695.

Wyllie, M.R.J., A.R. Gregory, and G.H.F. Gardner (1958), An experimental investigation of factors affecting elastic wave velocities in porous media, Geophys., 23, 459-493.